ANALYSIS AND EXPERIMENTAL EVALUATION OF AN ULTRA-HIGH TEMPERATURE PYROLYTIC GRAPHITE THERMOCOUPLE

C. A. KLEIN

M. P. LEPIE

R. N. DONADIO

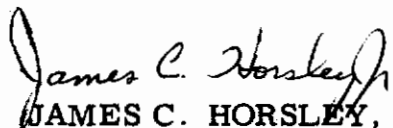*** Export controls have been removed ***

FOREWORD

This report was prepared by Raytheon Company, Research Division, Waltham, Massachusetts, on Air Force Contract AF 33(615)-2650. The work was supervised and this report was prepared by C. A. Klein, M. P. Lepie, and R. N. Donadio. The contract was initiated under Project No. 1469, "Vehicle Loads Validation", Task No. 146907, "Advanced Technology for Data Sensing". The work described in this document was authorized by and completed under the auspices of the Air Force Flight Dynamics Laboratory, Research and Technology Division, with Mr. William P. Johnson as Project Engineer.

This report covers work conducted from May 1965 to November 1965.

This Manuscript was released by the authors in December 1965 for publication as a RTD Technical Report.

This technical report has been reviewed and is approved.

JAMES C. HORSLEY, JR.
Major, USAF
Chief, Experimental Mechanics Branch

ABSTRACT

This report is made up of three segments as follows:

1. A theoretical analysis of thermoelectricity along graphite layer planes is presented. It is shown how the thermo-electric power (TEP) can be derived from the Slonczewski-Weiss description of the graphite band structure. From the density of state equation rigorous indications on the energy dependence of the scattering parameter were derived, permitting valid comparisons with experimental results to be made.

2. Chapter II summarizes the experimental procedure. Great care was taken in order to arrive at reliable Seebeck coefficients. Thermocouple work was plagued by experimental difficulties (furnace conductance) of a similar nature as experienced by other investigators.

3. Finally, measured TEP was assessed in the light of the theory developed in Chap. I. New light was thus shed upon critical parameters such as the mobility ratio, leading to a much improved description of transport in pyrolytic graphite and alloys of pyrolytic graphite. It was demonstrated that BPG/PG thermocouples are intrinsically capable of delivering exceptionally favorable output characteristics; a reduction to practice will require further efforts, in particular in connection with proper test furnace design.

TABLE OF CONTENTS

LIST OF ILLUSTRATIONS

v

I. THEORETICAL CONSIDERATIONS

A. General Introduction

In this section we summarize elements of the formal theory of conduction relevant to the problem in hand; treatment and notations are as in Wilson's book.[1]

A wave vector $\underline{k}$ is used to define the electron states, and the number of electrons per unit volume whose wave vectors lie in an element d^3k is

$$(1/4\pi^3)\, f\ (\underline{k},\ \underline{r})\ d^3 k \tag{1}$$

In equilibrium $f(k, r)$ is the Fermi function $f_o\ (E)$. In the presence of external fields, or a temperature gradient, the distribution function must be determined from the Boltzmann equation, which is as follows:

$$(-e/\hbar)\ (\ \underline{\xi}\ +\ \underline{v}\,\mathcal{H}/c)\ \nabla_{\underline{k}} f + \underline{v} \cdot \nabla\ f\ = [\frac{\partial f}{\partial t}]_{coll} \tag{2}$$

Here, $[\partial f/\partial t]_{coll}$ is the rate of charge of due to interactions with the lattice or other scatterers. We shall make the assumption that $[\partial f/\partial t]_{coll}$ can be taken to be of the form

$$[\partial f/\partial t]_{coll}^{\cdot}\ =\ -(f-f_o)/\tau \quad , \tag{3}$$

where τ is the usual "relaxation time". At this stage no assumptions need be made about τ or E, and it will be sufficient to consider the case in which only one band is present.

To find the electrical conductivity in a uniform sample we put $\mathcal{H} = 0$ and $\nabla_r f = 0$ in Eq. (2). Since the electrical field in a conductor is always small, we may neglect terms in E^2 and thus obtain the solution of (2) by putting $f = f_o$ on the left of the equation. Using the relationship $\nabla_k E = \hbar v$, one gets:

$$f = f_o + (e/\hbar) \tau \, \mathcal{E} \, \nabla_k f_o = f_o + e \tau \, v \cdot \mathcal{E} \, \partial f_o / \partial E \qquad . \qquad (4)$$

The electric current density J is then given by

$$J = - \frac{e}{4\pi^3} \int_{BZ} v f d^3 k = \frac{e^2}{4\pi^3} \int_{BZ} \tau v \, (v \cdot \mathcal{E}) (- \frac{\partial f_o}{\partial E}) \, d^3 k \qquad . \qquad (5)$$

Using tensor notations, we see that the conductivity tensor σ_{ij} is given by

$$\sigma_{ij} = \frac{e^2}{4\pi^3} \int_{BZ} \tau v_i \, v_j \cdot (- \frac{\partial f_o}{\partial E}) \, d^3 k \qquad . \qquad (6)$$

The integration must be carried out by considering elements of k space as they relate to the appropriate Brillouin zone (BZ).

On open circuit, the heat flow produced by a temperature gradient results in a redistribution of the charge carriers so as to set up an electric field of the right amount to counteract the drift of the carriers and to reduce the electric current to zero. In the layer planes of graphite the generated electric field is in the same direction as the temperature gradient, which we take to be along the u axis, and the Boltzmann equation is then

$$- \frac{e}{\hbar} \, \mathcal{E} \frac{\partial f}{\partial k_x} + v_x \frac{\partial f}{\partial x} = - \frac{f - f_o}{\tau} \qquad . \qquad (7)$$

2

As before, we may obtain a solution of (7) by putting $f = f_o$ on the left-hand side. Since $\partial f_o / \partial x = (\partial f_o / \partial T)(\partial T / \partial x)$ and

$$\frac{\partial f_o}{\partial T} = T \frac{\partial}{\partial T} \left(\frac{E - E_F}{T} \right) \frac{\partial f_o}{\partial E} \quad , \tag{8}$$

it follows that

$$f = f_o + \tau v_x \frac{\partial f_o}{\partial E} \left[\mathcal{E}_x + T \frac{\partial}{\partial x} \left(\frac{E_F}{T} \right) + \frac{E}{T} \frac{\partial T}{\partial x} \right] \quad . \tag{9}$$

Hence, for $J_x = 0$, one has

$$0 = - \frac{e}{4\pi^3} \int_{BZ} v_x f d^3 k = K_1 \left[e^2 \mathcal{E}_x + eT \frac{\partial}{\partial x} \left(\frac{E_F}{T} \right) \right] + K_2 \frac{e}{T} \frac{\partial T}{\partial x} \, , \tag{10}$$

where

$$K_1 = \frac{1}{4\pi^3} \int_{BZ} \tau v_x^2 \left(- \frac{\partial f_o}{\partial E} \right) d^3 k = \sigma_{2x} / e^2 \quad , \tag{11}$$

and

$$K_2 = \frac{1}{4\pi^3} \int_{BZ} \tau v_x^2 \, E \left(- \frac{\partial f_o}{\partial E} \right) d^3 k \tag{12}$$

Equation (10) shows that the electric field $\mathcal{E}_x$ is given by

$$-e \mathcal{E}_x = \frac{\partial E_F}{\partial x} + \frac{\partial T}{\partial x} \left(\frac{K_2}{T K_1} - \frac{E_F}{T} \right) \quad , \tag{13}$$

and thus that the absolute thermoelectric power (Seebeck coefficient) as usually defined is

$$\boxed{ Q = - \frac{k}{e} \left(\frac{K_2}{kT K_1} - \frac{E_F}{kT} \right) } \tag{14}$$

3

B. Graphite Band Structure and Carrier Scattering Model

Graphite has a layered hexagonal structure. Within a layer the atoms are distributed in hexagonal sites and are bound to one another by very strong covalent bonds. The distance between the atoms in a layer is 1.42Å, and the lattice parameter is a_o = 2.46Å. The layers are weakly bound to one another and the distance between them is 3.35Å. In the adjacent layer the atoms are displaced so that the center of a hexagon lies above an atom of the lower layer. The period along the hexagonal axis c_o is actually 6.70Å. The Brillouin zone of graphite (see Fig. 1) is therefore a six-sided prism with a base of side $2\pi/a_o$ and a height (edge) $2\pi/c_o$. Charge carriers occupy a narrow region near the Brillouin zone edge, and the transverse dimensions of this region amount to about one percent of $2\pi/a_o$. The energy of the carriers depends on the momentum components k_z and κ (the distance from an edge of the BZ) in a manner initially described by Slonczewski and Weiss.[2] For the purpose of investigating transport in pyrolytic graphite (polycrystalline material) we consider it a fair approximation to restrict one's attention to the majority carriers, or more precisely, to an electron band

$$E_e = 2\gamma_2 \cos^2 (\xi/2) + \hbar^2 \kappa^2 / 2m^*(\xi) \quad , \tag{15}$$

and a hole band (inverted band)

$$E_h = 2\gamma_2 \cos^2 (\xi/2) - \hbar^2 \kappa^2 / 2m^*(\xi) \quad . \tag{16}$$

Then, $\xi = k_z c_o$ and the effective mass is

$$m^*(\xi) = (4/3)(\hbar/a_o)^2 (\gamma_1/\gamma_o^2) \cos (\xi/2) \quad . \tag{17}$$

Note that γ_o (≈ 2.8 eV) characterizes interactions in the layer planes. The parameter γ_1 (≈ 0.27 eV) characterizes the overlapping of wave functions of neighboring nonequivalent layers, while γ_2 (≈ 0.015 eV) represents the interaction of equivalent layers separated by a distance c_o from one another.

4

N-TYPE PG

P-TYPE PG

E — upper π band —

E_0 — Fermi

Energy —

— lower π band —

k_z

$+\pi/c_0$

O κ

$-\pi/c_0$

STB model

$E_h = E_0 - \hbar^2 \kappa^2/2m^*$

$E_e = \hbar^2 \kappa^2/2m^*$

STB model

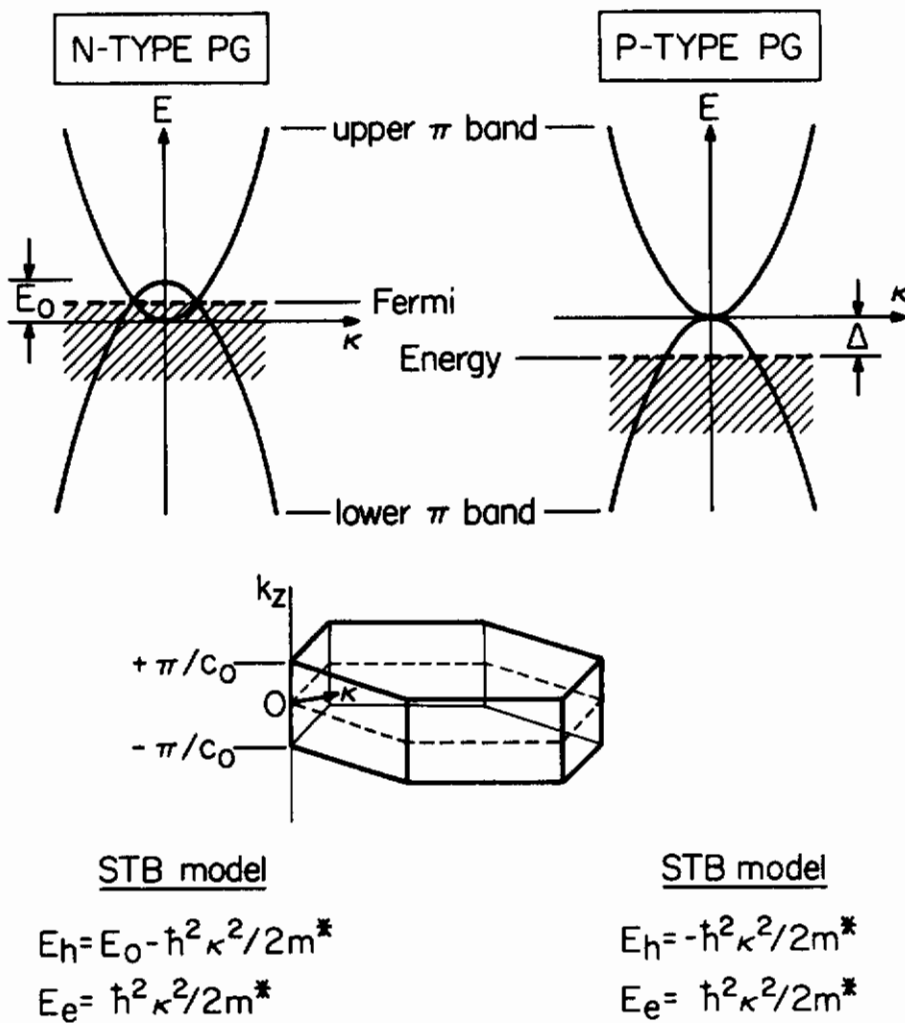$E_h = -\hbar^2 \kappa^2/2m^*$

$E_e = \hbar^2 \kappa^2/2m^*$

Figure 1   The Brillouin Zone of Graphite

5

First we wish to consider in detail the evaluation of the number of the number of free carriers. In the light of (1) the number of electrons and holes per unit volume is given by

$$n_o = \frac{1}{4\pi^3} \int_{BZ} f_o d^3k \quad \text{and} \quad n_h = \frac{1}{4\pi^3} \int_{BZ} (1-f_o) d^3k \quad , \quad (18)$$

where f_o is the usual Fermi distribution function

$$f_o = \left\{ \exp (E-E_F)/kT + 1 \right\}^{-1} \quad . \quad (19)$$

After substituting

$$2\pi \kappa d\kappa dk_z = (\pi/c_o) d(\kappa^2) d\xi \quad (20)$$

for d^3k and taking into account spatial degeneracy (there are two vertical BZ edges that must be considered), it follows that

$$n_e = \frac{1}{2\pi^2 c_o} \int_{-\pi}^{+\pi} d\xi \int_0^\infty f_o d(\kappa^2) = \frac{1}{2\pi^2 c_o} \int_{-\pi}^{+\pi} d\xi \int_{E_o(\xi)}^\infty \kappa^2 (-\frac{\partial f_o}{\partial E}) dE \quad , \quad (21)$$

and

$$n_h = \frac{1}{2\pi^2 c_o} \int_{-\pi}^{+\pi} d\xi \int_0^\infty (1 - f_o) d(\kappa^2) = \frac{1}{2\pi^2 c_o} \int_{-\pi}^{+\pi} d\xi \int_{-\infty}^{E_o(\xi)} \kappa^2 (-\frac{\partial f_o}{\partial E}) dE \quad . \quad (22)$$

In writing (21) and (22) we are referring to the band system (15) and (16), which may also be described by

$$\kappa^2 = (\pi/\hbar^2) \langle m^* \rangle \cos(\xi/2) |E-E_o(\xi)| \quad , \quad (23)$$

6

where $\langle m^* \rangle$ represents an "average effective mass"

$$\langle m^* \rangle = (8/3\pi) (\hbar/a_o)^2 (\gamma_1/\gamma_o^2) \quad , \tag{24}$$

and $E_o(\xi)$ stands for $2\gamma_2 \cos^2(\xi/2)$. From Eqs. (21) to (23) we deduce that the total carrier density is

$$n_e + n_h \equiv \frac{\langle m^* \rangle}{2\pi\hbar^2 c_o} \int_{-\pi}^{+\pi} d\xi \cos(\xi/2) \int_{-\infty}^{+\infty} | E - E_o(\xi) | (-\frac{\partial f_o}{\partial E}) dE \tag{25}$$

in accordance with the result of Arkhipov, et al.[3] In the case of pure graphite ($n_e = n_h$), these authors have shown that the integral (25) becomes independent of γ_2 when $kT > \gamma_2$. Since we are primarily concerned with temperatures in the range above 300° K, we conclude that for all practical purposes we may set $E_o(\xi) = 0$, or in other words, ignore the effects of "overlap" in the frame of this work. It is then a straightforward matter to derive analytical expressions for the electron and the hole concentration in various classes of pyrolytic graphite (PG):

$$n_e = \frac{\langle m^* \rangle}{2\pi h^2 c_o} \int_{-\pi}^{+\pi} \cos(\xi/2) d\xi \int_0^\infty E(-\frac{\partial f_o}{\partial E}) dE = \frac{2\langle m^* \rangle}{\pi h^2 c_o} kT \, F_o(\frac{E_F}{kT})$$

$$\tag{26}$$

$$n_h = \frac{\langle m^* \rangle}{2\pi h^2 c_o} \int_{-\pi}^{+\pi} \cos(\xi/2) d\xi \int_{-\infty}^0 |E| (-\frac{\partial f_o}{\partial E}) dE = \frac{2\langle m^* \rangle}{\pi h^2 c_o} kT \, F_o(-\frac{E_F}{kT}) \quad .$$

Here, F_o designates the Fermi-Dirac integral of order $j = 0$, and E_F is the Fermi energy. Note that for graphitized PG one has $E_F = 0$, while in turbostratic (as-deposited) or boronated specimens $E_F = -\Delta$, if Δ measures the Fermi-level depression.[4]

7

At this point proper attention must be given to the scattering mechanism. Following McClure,[5] we assume that a relaxation time τ exists and may be approximated by the "golden rule" for transition probabilities:

$$\tau^{-1} = (2\pi/\hbar)|V|^2 N(E) \quad .$$

(27)

Here, V is the matrix element of the scattering potential, and $N(E)$ is the density of final states. Theories of electron scattering have shown that V is independent of $\mathbf{k}$ and E for small changes in $\mathbf{k}$. As far as graphite is concerned, this requirement is met for changes of the $\mathbf{k}$ vector perpendicular to the $\underline{c}$ axis. Within the approximation $\gamma_2 = 0$, we may thus assume that V is independent of energy, and hence that the density of states characterizes the scattering process. The density of states is given by

$$N(E)\, dE = \frac{1}{4\pi^3} \int d^3 k \quad ,$$

(28)

where the integral is taken over the part of k space lying between the contours E and $E + dE$. In the light of Eq. (26) it is seen that

$$N(E)\, dE = \frac{2\langle m^*\rangle\, dE}{\pi k^2 c_o} \quad ,$$

(29)

or in other words, that we are dealing with a constant density-of-states situation, and hence that we have relaxation times which are energy independent. Note that McClure[5] defines separate deformation potential constants for electrons and for holes (D_e and D_h); in consequence our scattering model involves two constant relaxation times τ_e and τ_h.

8

C. The Thermoelectric Power

If we write σ_e and Q_e for the electron contribution to conductivity and thermoelectric power, assuming a single electron band, and similarly σ_h, Q_h for the contribution from the holes in the absence of electrons, we have

$$Q_{\parallel} = \frac{\sigma_e Q_e + \sigma_h Q_h}{\sigma_e + \sigma_h} \tag{30}$$

for the layer-plane TEP of graphite.[6] We now wish to evaluate the various components entering Eq. (30) from the formal theory presented in Section A and the graphite model developed in Section B. According to (6), the layer-plane conductivity due to electrons is

$$\sigma_e = \frac{e^2}{4\pi^3} \int_{BZ} \tau_e v_x^2 \left(-\frac{\partial f_o}{\partial E}\right) d^3k = \frac{e^2}{2\pi^2 c_o} \int_{-\pi}^{+\pi} d\xi \int_0^{\infty} \tau_e v_x^2 \left(-\frac{\partial f_o}{\partial E}\right) d(\kappa^2) . \tag{31}$$

In our approximation the surfaces of constant energy are figures of rotation about the vertical zone edge, so that we may replace v_x^2 in the integral by $v^2/2$, where

$$v = \frac{1}{\hbar} \frac{\partial E}{\partial \kappa} = \frac{2\kappa}{\hbar} \cdot \frac{\partial E}{\partial (\kappa^2)} . \tag{32}$$

With $E_e = \hbar^2 \kappa^2 / 2m^*(\xi)$, it follows that

$$\sigma_e = \frac{e^2}{\pi^2 \hbar^2 c_o} \int_{-\pi}^{+\pi} d\xi \int_0^{\infty} \tau_e E \left(-\frac{\partial f_o}{\partial E}\right) dE = \frac{2e^2 \tau_e}{\pi \hbar^2 c_o} kT F_o \left(\frac{E_F}{kT}\right) . \tag{33}$$

As expected, it turns out that $\sigma_e = e n_e \mu_e$, where $\mu_e = e\tau_e / \langle m^* \rangle$ (see Eq. 26). By the same token we have

$$\sigma_h = e n_h \mu_h = \frac{2e^2 \tau_h}{\pi \hbar^2 c_o} kT F_o \left(-\frac{E_F}{kT}\right) . \tag{34}$$

9

In Section A it was shown that the Seebeck coefficient for a single electron band is

$$Q_e = -\frac{k}{e} \left(\frac{K_{2,e}}{kTK_{1,e}} - \frac{E_F}{kT} \right) \tag{35}$$

where $K_{1,e} = \sigma_e / e^2$ and

$$K_{2,e} = \frac{1}{4\pi^3} \int_{BZ} \tau_e v_x^2 E \left(-\frac{\partial f_o}{\partial E} \right) d^3 k \qquad . \tag{36}$$

Proceeding in the same manner as with the conductivity, one finds

$$K_{2,e} = \frac{1}{\pi^2 h^2 c_o} \int_{-\pi}^{+\pi} d\xi \int_o^\infty \tau_e E^2 \left(-\frac{\partial f_o}{\partial E} \right) dE = \frac{4\tau_e}{\pi h^2 c_o} (kT)^2 F_1 \left(\frac{E_F}{kT} \right), \tag{37}$$

since

$$\int_o^\infty E^2 \left(-\frac{\partial f_o}{\partial E} \right) dE = 2 (kT)^2 F_1 (E_F / kT) \qquad , \tag{38}$$

where F_1 designates the Fermi-Dirae integral of order 1. We conclude that

$$Q_e = -\frac{k}{e} \left[\frac{2F_1 (E_F / kT)}{F_o (E_F / kT)} - \frac{E_F}{kT} \right] \tag{39}$$

and, similarly, for the inverted band one has

$$Q_h = \frac{k}{e} \left[\frac{2F_1 (-E_F / kT)}{F_o (-E_F / kT)} + \frac{E_F}{kT} \right] \qquad . \tag{40}$$

(Note that in Eq. (40) the sign is inverted since the thermoelectric effect depends upon the first power of the electric charge.)

10

In terms of the usual carrier-density and carrier-mobility ratios a and b,

$$a = \frac{n_h}{n_e} = \frac{F_0(\Delta/kT)}{F_0(-\Delta/kT)} \qquad (41a)$$

$$b = \frac{\mu_e}{\mu_h} = \frac{\tau_e}{\tau_h} \qquad , \qquad (41b)$$

it follows from Eq. (30) that $Q_{||} = (a Q_h + b Q_e)/(a + b)$ and thus that we may calculate the Seebeck coefficient of a pyrolytic graphite specimen simply by writing:

$$Q_{||} = \frac{k}{e} \left[\frac{a}{a + b} (\delta_+ - \frac{\Delta}{kT}) - \frac{b}{a + b} (\delta_- + \frac{\Delta}{kT}) \right] \qquad , \qquad (42)$$

where

$$\delta_\pm = \frac{2F_1(\pm\Delta/kT)}{F_0(\pm\Delta/kT)} \qquad . \qquad (43)$$

and Δ measures the Fermi-level depression ($\Delta = - E_F$). All subsequent numerical work rests on this expression and does not involve any further assumption.

11

II. EXPERIMENTAL PROCEDURE

A. Seebeck Coefficient

Thomson[7] has derived the thermodynamic equation

$$\frac{de_{1,2}}{dT} = \frac{\sigma_1 - \sigma_2}{T} \quad ,$$

(1)

where $e_{1,2}$ is the thermoelectric force per degree and σ_1, σ_2 Thomson coefficients of the two components that make up a given thermocouple. T is the absolute temperature.

Nernst[8] has shown that $e_{1,2}$ and σ approach zero with T in such a way that Eq. (1) can be integrated

$$e_{1,2} = \int_0^T \frac{\sigma_1}{T} dT - \int_0^T \frac{\sigma_2}{T} dT \quad .$$

(2)

By definition,[9] the absolute thermoelectric force (Seebeck coefficient, e, of a substance is

$$e = \int_0^T \frac{\sigma}{T} dT \quad .$$

(3)

Therefore, combining Eq. (2) with Eq. (3)

$$e_{1,2} = e_1 - e_2 \quad .$$

(4)

12

Using the relationship in Eq. (4) it is possible to determine the
absolute Seebeck coefficient of a given material provided its thermoelectric
force per degree is measured against a second material whose absolute
Seebeck coefficient is known.

We have chosen to use pure platinum as the other material in our
PG thermocouple in order to find the absolute Seebeck coefficient of PG
and its boron alloys. Platinum can be obtained in extremely pure wires
that are inert to graphite up to 1400°C. Most importantly, the Seebeck
coefficient of platinum[10] is known to 900°C. We have estimated values above
900°C by extrapolation because the curve of Seebeck coefficient vs tempera-
ture is linear from 400° to 900°C.

Figure 2 is a sectional drawing of the furnace used to produce
a thermal gradient along the test specimen. Figure 3 shows the sample
in more detail along with a wiring diagram of the measurements circuit.
The furnace consists of two individually controlled platinum-20 percent
rhodium heaters which are concentric with each other but displaced along
their common axis so that a thermal gradient was produced. A stable ΔT
of 5° − 15°C along the sample was achieved within one half hour. No prob-
lems were encountered with the operation of the furnace or its controls.

The Seebeck coefficient specimens was made of a PG bar approxi-
mately $1/4 \times 1/4 \times 5$ in. Pure platinum and Pt/10% Rh wires (10 mil diam)
were inserted into holes in the sample. The holes were about three inches
apart. Figure 3 shows which wires were used to measure the ΔT between
holes, the temperature T, at one hole and the emf created by the ΔT for a
Pt/PG thermocouple. The current created by the thermocouple was sent
through a Leeds & Northrup DC Amplifier No. 9835 A and a Keitheley DC
Microvoltmeter No. 150 AR and then fed into a Leeds & Northrup 6-point
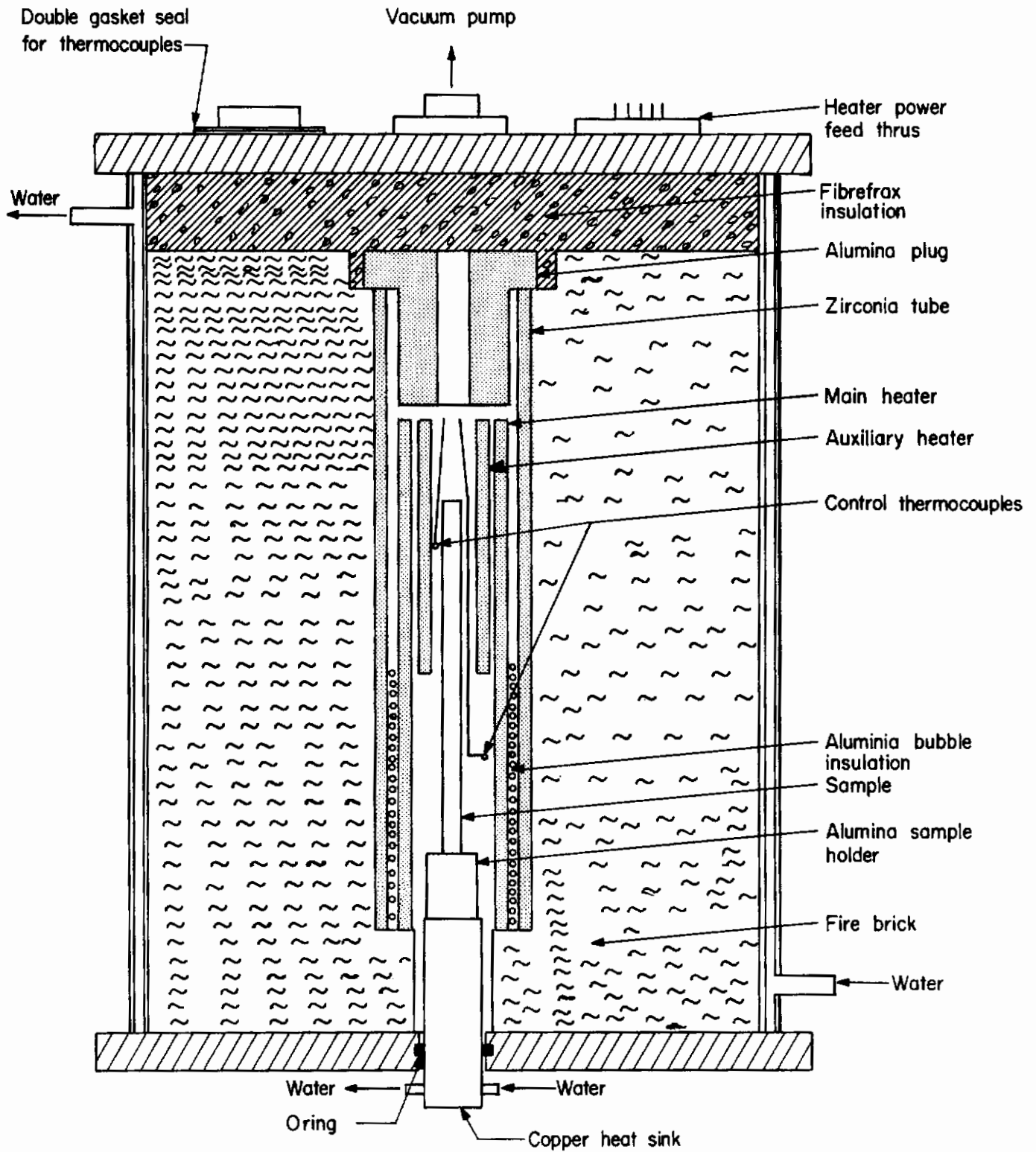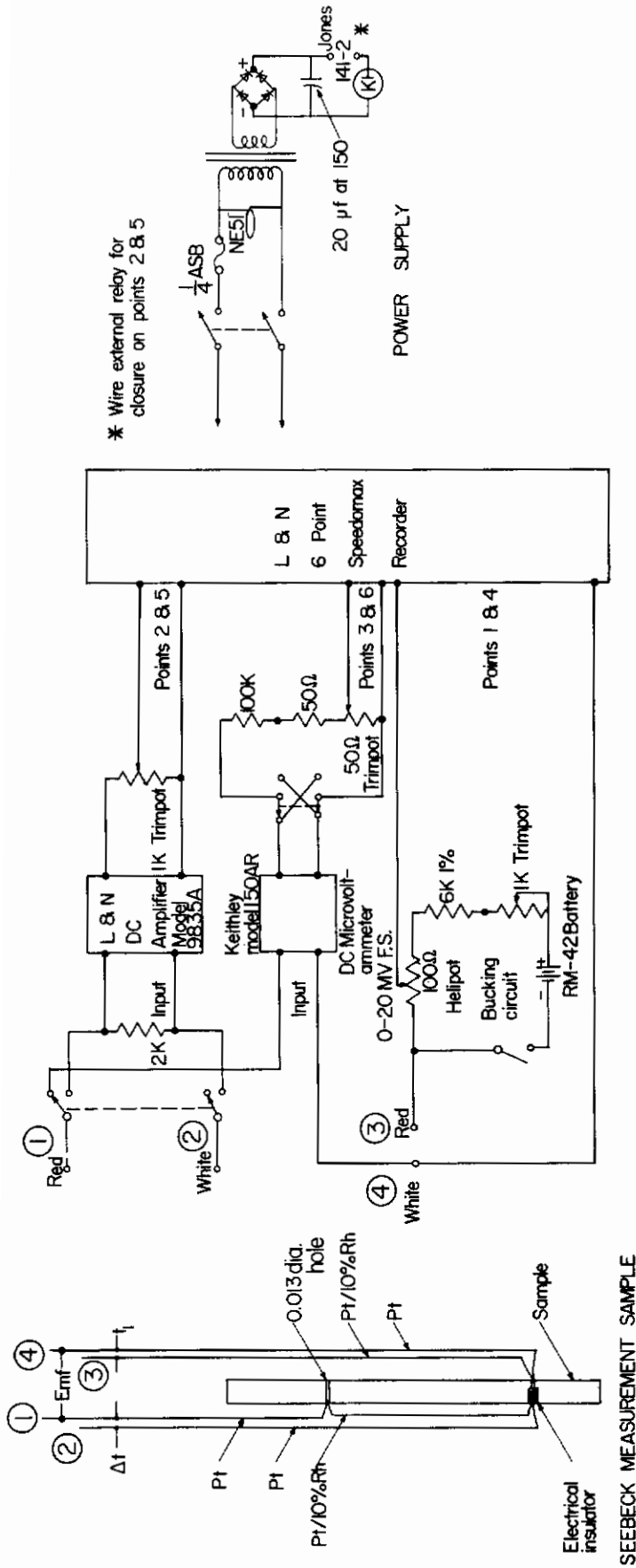Speedomax Recorder.

Figure 2   Seebeck Measurement Apparatus

14

Figure 3   Wiring Diagram for Seebeck Coefficient Apparatus

15

Some sources of error in the initial measurements were recognized and corrected with little difficulty. Contact of lead wires in the PG holes was lost frequently until the platinum wedges were replaced by rivets to which the wires were spot welded. The rivets were made by inserting platinum tubing into the holes in the PG and then peening over the ends of the tube. Leakage of current through the 94 percent alumina insulators above 900°C was cured (up to 1100°C) by replacement with insulators of 99 percent alumina. The a.c. pickup from the heaters was avoided by turning them off momentarily during measurements. Finally, electronic feedback, caused by the three signals going through the complex circuit in rapid succession, was cured by using three separate microvoltmeters.

Oxidation of the PG and BPG test specimens because of small leaks in the "vacuum" furnace were observed to increase the absolute Seebeck coefficient. Thus, successive runs on the sample resulted in Seebeck curves that were displaced upward when leaks were undetected.

One difficulty that could not be overcome was the inhomogeneity in the BPG samples. Variations in composition were found especially along the length of the sample. This was most evident for small concentrations of boron.

Another variation was the degree of heat treatment for the long PG thermocouple rods. Portions of the rod fired in the center of the heat-treat furnace were so highly graphitized that they became soft while this was not true for the portions at either end. Since the Seebeck coefficient of graphite is highly sensitive to the degree of graphitization this variation could cause different results depending on where the sample was cut from the long rod. Every effort was made to use only the part that was highly graphitized.

16

B. Thermocouples

When two materials, 1 and 2, are joined together in a loop and a voltage, V_o, applied while one junction is hot and the other cold, the circuit is found to contain an additional voltage (Seebeck voltage)

$$e.\,m.\,f. = V_o - V_{1,2} \qquad .\qquad (5)$$

The Seebeck coefficient for materials 1 and 2 is

$$e_{1,2} = dV_{1,2}/dT_h \qquad . \qquad (6)$$

By adjusting V_o to zero current, then $V_{1,2} = V_o$ and thus the Seebeck voltage and coefficient are measured.

Figure 4 is a schematic of the initial apparatus used to measure the PG-BPG thermocouple. Rods of the two substances were inserted into a graphite block. The opposite ends of the rods were copper plated and brazed to copper lead wires. The plated end was water cooled while the end with the graphite block was suspended in the center of a resistance heated graphite furnace. Temperature at the hot end was determined by a Pt-Pt/10%Rh couple up to its melting point and above this by sighting into a hole in the block with an optical pyrometer. Cold junction temperature was found by a Cu-Constantan couple inserted in a test rod.

The major difficulty here was the same one which plagued our earlier thermocouple measurements. As the temperature of the furnace rose above about 1900°C the thermoelectric current dropped off and the resistance between the furnace wall and the thermocouple went from infinite to only a few ohms at about 2300°C. The nitrogen atmosphere in the furnace had become increasingly conductive, electronically, with the increase in temperature. Since the ionization potential of helium is higher

17

Water in

Water out

Furnace cover

Flexible hose

Copper plated ends

Water cooled copper jacket

Boron PG leg

Radiation shielding

Test thermocouple

Graphite test block

Sight hole

Copper } emf leads
Copper

Copper } Reference temperature
Constantan } leads

PG leg

Pyrex tubes packed with cement

Platinum

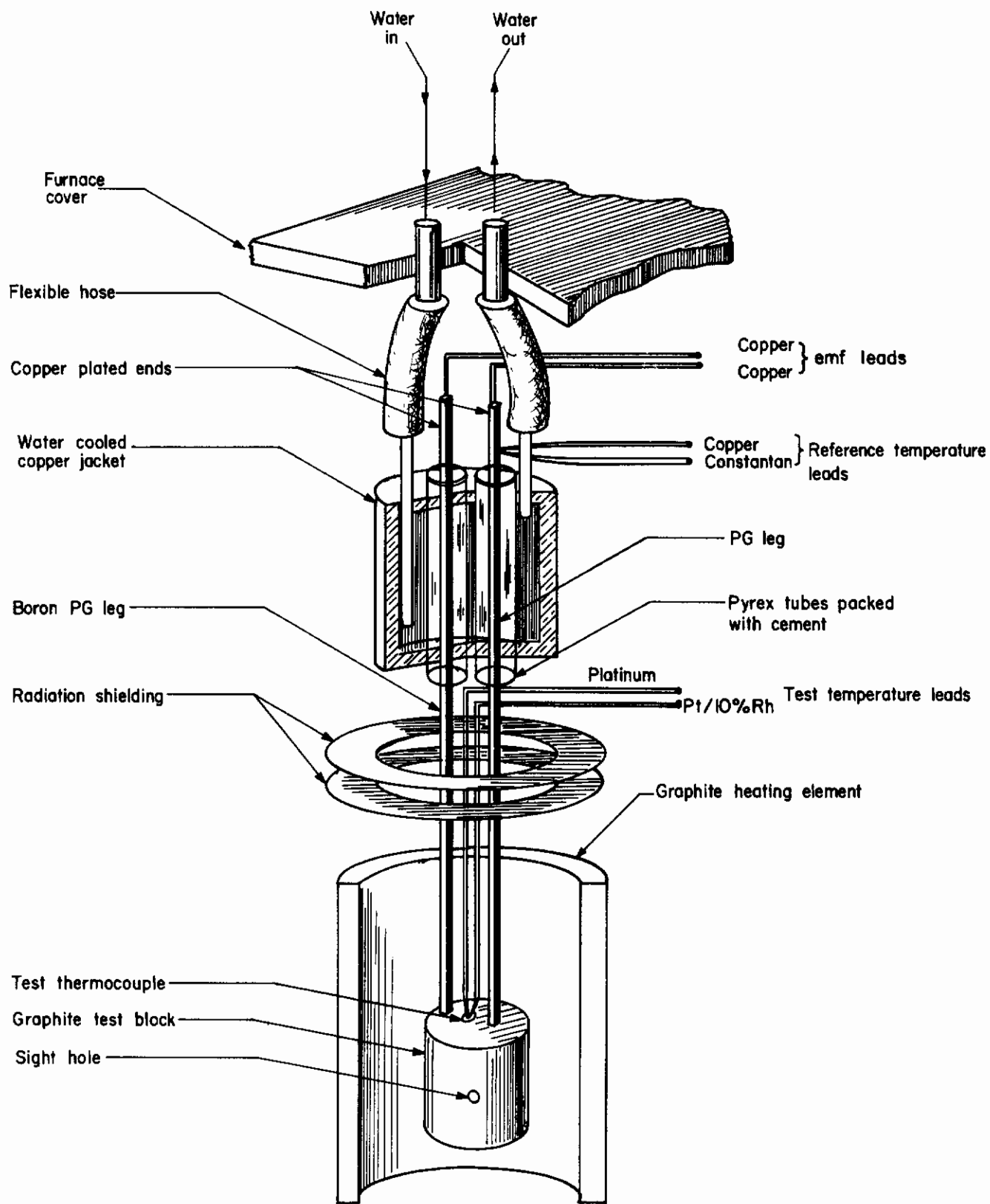Pt/10%Rh   Test temperature leads

Graphite heating element

Figure 4   Thermocouple Test Apparatus

18

than that of other gases it was used to replace nitrogen. This resulted in a positive thermoelectric current up to about 2400°C in place of 2000°C for 2 mm Hg nitrogen. Another scheme attempted in an effort to alleviate electrical leakage to ground was to set the thermocouple rod at 180° to each other instead of parallel as shown in Fig. 4. The increased leakage path did little to reduce the conductance to ground at elevated temperatures. It was hoped to increase further the high temperature potential of the thermo- couple by using a solid insulator of vapor deposited boron nitride. Unfor- tunately the program's time limitation did not permit this additional experi- mentation. The program did show, however, that within the limitations of gas or ceramic insulation the PG-BPG thermocouple can operate as high in temperature as the more conventional W/W-Re thermocouple and deliver a much higher thermoelectric voltage.

19

III. DATA AND RESULTS

Our goal is to describe the thermoelectric behavior of pyrolytic graphites at high temperature. In Chapter I we have seen that the Seebeck coefficient of graphite (layer-plane transport) is given by

$$Q_{\parallel} = \frac{k}{e} \left[\frac{a}{a+b} \left(\delta_+ - \frac{\Delta}{kT} \right) - \frac{b}{a+b} \left(\delta_- + \frac{\Delta}{kT} \right) \right] \qquad , \qquad (1)$$

where k is the Boltzmann constant, e the electronic charge,[*] a the carrier-concentration ratio, b the carrier-mobility ratio, Δ the Fermi-level depression, and T the absolute temperature. Moreover, it was established that

$$\delta_{\pm} = \frac{2 \mathscr{F}_1 (\pm \Delta/kT)}{\mathscr{F}_0 (\pm \Delta/kT)} \qquad , \qquad (2)$$

where $\mathscr{F}_j (\mathfrak{X})$ is a Fermi integral:

$$\mathscr{F}_j (\mathfrak{X}) = \frac{1}{\Gamma(j+1)} \int_0^{\infty} \frac{\epsilon^j \, d\epsilon}{1 + \exp(\epsilon - \mathfrak{X})} \qquad (3)$$

$\Big[$These integrals are tabulated in Appendix B of J. S. Blakemore's Semi-conductor Statistics (Pergamon Press, New York, 1962).$\Big]$ Since

$$a = \frac{\ln[1 + \exp(+ \Delta/kT)]}{\ln[1 + \exp(- \Delta/kT)]} \qquad (4)$$

and $b = \tau_e/\tau_h$, it follows that the Seebeck coefficient as formulated in Eq. (1) should be completely determined by the Fermi-level depression Δ and the relaxation time ratio b. In the light of the experiments described in Section II we will now investigate the validity of our approach to thermo-electricity in graphite at high temperatures.

----

[*]Note that $k/e = 86.4 \ \mu V/°C$.

A. Graphitized PG

Highly heat-treated pyrolytic graphite is known to exhibit "intrinsic" semimetallic characteristics, or in other words, to have electron and hole concentrations that are roughly identical over the whole temperature range. In consequence, we may assume a $\approx$ 1, which implies $\Delta \approx 0$ considering thar our model ignores band-overlap effects. Under these conditions Eqs. (1) and (2) yield

$$Q_{\|} = \frac{k}{e} \left[\frac{1-b}{1+b}\right] \frac{2 \mathscr{F}_1(0)}{\mathscr{F}_0(0)} \qquad . \qquad (5)$$

Since $k/e = 86.4 \,\mu V/°C$ and $2 \mathscr{F}_1(0)/\mathscr{F}_0(0) = 2.37$, it follows that the Seebeck coefficient will be determined by the mobility ratio exclusively. In effect, Eq. (5) reveals that the Seebeck coefficient measured in the direction of the layer planes of graphitized PG yields direct information on the mobility ratio in near-ideal graphite. Previous galvanomagnetic experimentation failed to provide reliable indications concerning this most critical parameter. For this very reason substantial effort was devoted at assessing b from Seebeck coefficient measurements.

In Fig. 5 (left-hand side) we reproduce typical results of emf and TEP measurements performed on graphitized PG using platinum as a standard. A confrontation of these results is most instructive. We note, in particular, the emf extremes at approximately 250° and 700°C; they correspond to zeros in the TEP at 200° and 700°C. Moreover, we note the TEP minimum $(-1.5\mu V/°C)$ at 525°C, which reflects an inflection point in the emf at the same temperature. This is a gratifying state of affairs and illustrates the accuracy of our experimental techniques.

The absolute thermoelectric power of platinum at high temperatures has been reported by a number of authors, most recently by Cusack and Kendall.[11] From their measurements we derived the Seebeck coefficients
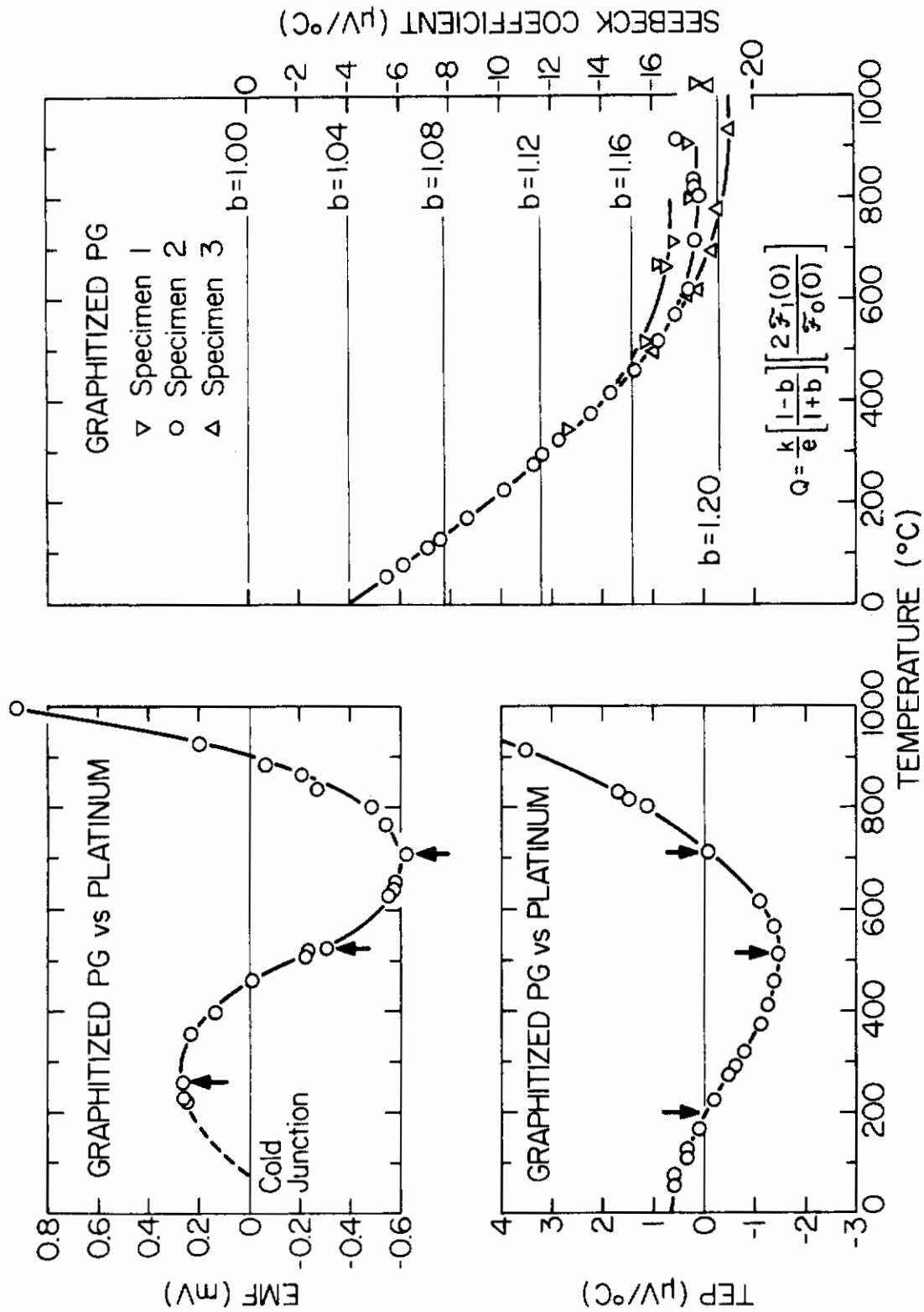
21

Figure 5   Thermoelectric Power of Highly Heat-Treated Pyrolytic
Graphite as Measured Along the Layer Planes

plotted on the right-hand side of Fig. 5. Three specimens heat-treated at approximately 3000 °C were considered. Up to about 500 °C, the Seebeck coefficient decreases at a fairly rapid rate (from about -5μV/ °C at room temperature to -15μV/ °C) more or less in accordance with the behavior observed at temperatures below 0 °C.[12] Above 500 °C, there is conclusive evidence of a plateau at about -18μV/ °C, but its exact location appears to be dependent upon the degree of graphitization of the specimen. This is a tentative conclusion, however, since TEP measurements at 1000 °C are poorly reproducible owing to the extreme sensitivity of the thermoelectric power of near-ideal graphite to surface oxidation.

In the light of Eq. (5) the Seebeck coefficient of graphitized PG points to a mobility ratio b that increases monotomically with temperature from about 1.05 at room temperature to about 1.20 at 1000 °C and above. The room temperature value turns out to be smaller than the commonly accepted 1.1 figure derived from Hall-effect studies; this may be attributed to imperfect graphitization of our test samples since near-ideal specimens yield Seebeck coefficients of about -10μV/ °C at room temperature.[12] Nevertheless, it can be stated that the measurements recorded in Fig. 5 demonstrate that the ratio remains between 1.0 and 1.2 over the whole temperature range in contrast to the preliminary indications reported in Ref. 13.

B. Turbostratic PG

Numerous investigations of turbostratic PG (pyrolytic graphite in its as-deposited configuration) have shown that crystalline defects associated with poor graphitization function as electron traps. Thus we must expect the Fermi level to be shifted into the valence band in a manner as illustrated in Fig. 6. If this is correct, the Seebeck coefficient at high temperatures must obey Eq. (1) with a Δ value characteristic of the number of traps. In Fig. 6 we have plotted curves obtained for Δ = 0.01, 0.015, and 0.02 eV,
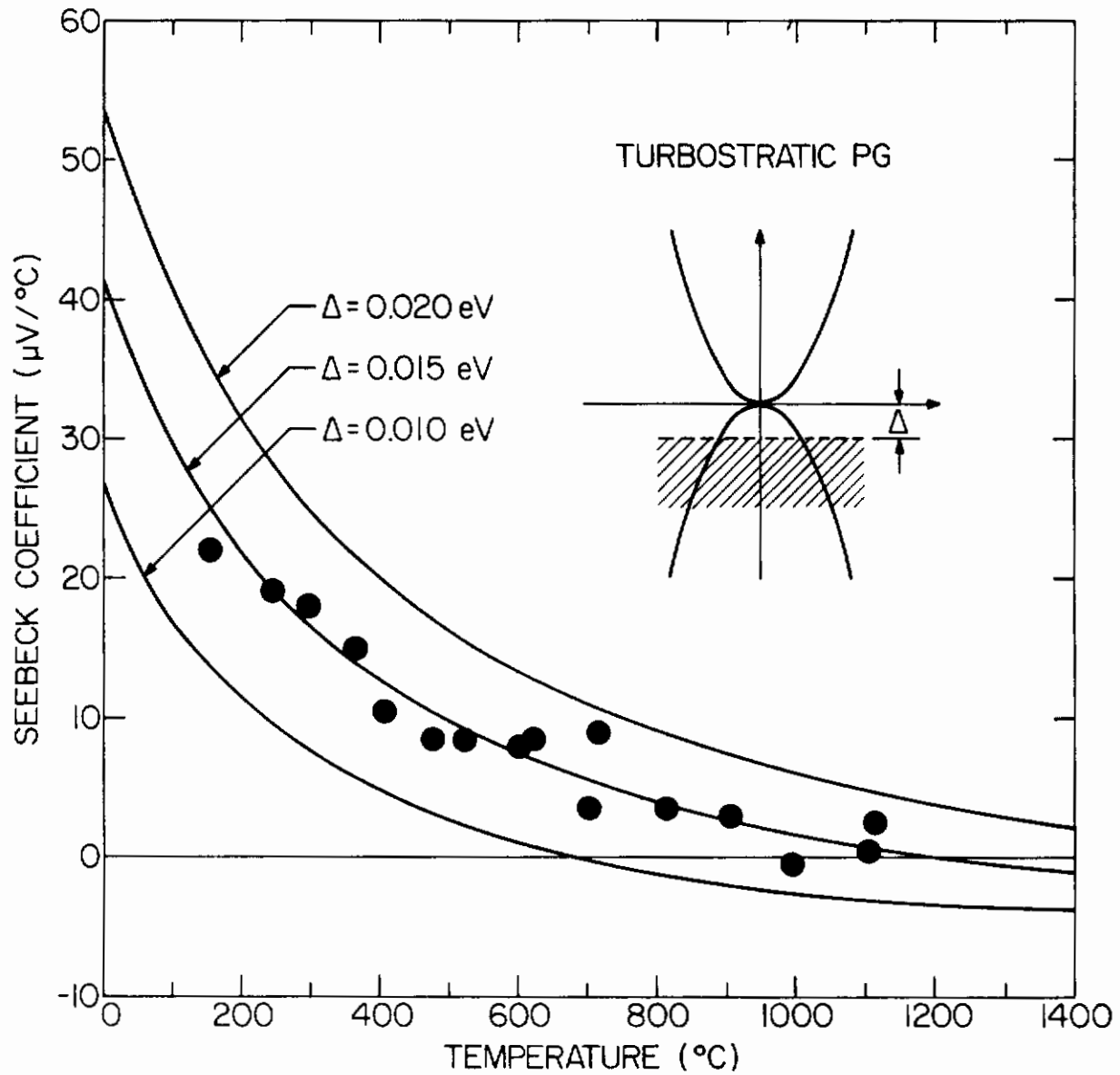
23

Figure 6   Thermoelectric Power of As-Deposited Pyrolytic Graphite
as Measured and Calculated in the Layer-Plane Direction

24

assuming a mobility ratio of 1.1.[*] (Note that, under these conditions, the thermoelectric power may change sign at very high temperatures.) On the same diagram are plotted Seebeck coefficients measured on a specimen deposited at 2100°C. It is seen that, above 2000°C, they decrease in fair agreement with predictions for a Fermi level depressed by 0.015 eV. For the sake of comparison we recall that Hall-effect measurements at room temperature indicate $\Delta \approx 0.02$ eV. We consider the discrepancy as minor, since a proper description of turbostratic PG at room temperature may involve band-overlap features that remain to be explored. In connection with turbostratic PG it must be emphasized that above 1000°C the Seebeck coefficient will become increasingly negative and should approach graphitized PG characteristics. It is concluded that a thermocouple junction made out of turbostratic and graphitized PG cannot function as a useful temperature sensor at very high temperatures. As reported in Chap. II, experimentation done along this line fully substantiates this conclusion: The device rapidly loses sensitivity above 1000°C, even though the net output is appreciable.

C. Boronated PG

Upon boronation the Fermi level shifts at a rapid rate into the valence band and we may first consider how this affects the Seebeck coefficient at a constant temperature. Figure 7 illustrates the situation at room temperature. The absolute TEP becomes rapidly positive, and a sharp peak develops at $\Delta \approx 0.05$ eV in response to the perturbation in the electron-hole balance. As the Fermi level shifts deeper into the valence band, however, a single carrier type situation evolves; with $\Delta/kT > 6$ the Seebeck coefficient exhibits a metallic-like behavior described by

$$Q_{\parallel} = Q_h = (k/2) (\pi^2/3) (kT/\Delta) \tag{6}$$

----

[*]In view of the complex scattering mechanism is turbostratic PG as compared to graphitized PG, the mobility ratios derived from Fig.5 can only be considered indicative of the true situation.
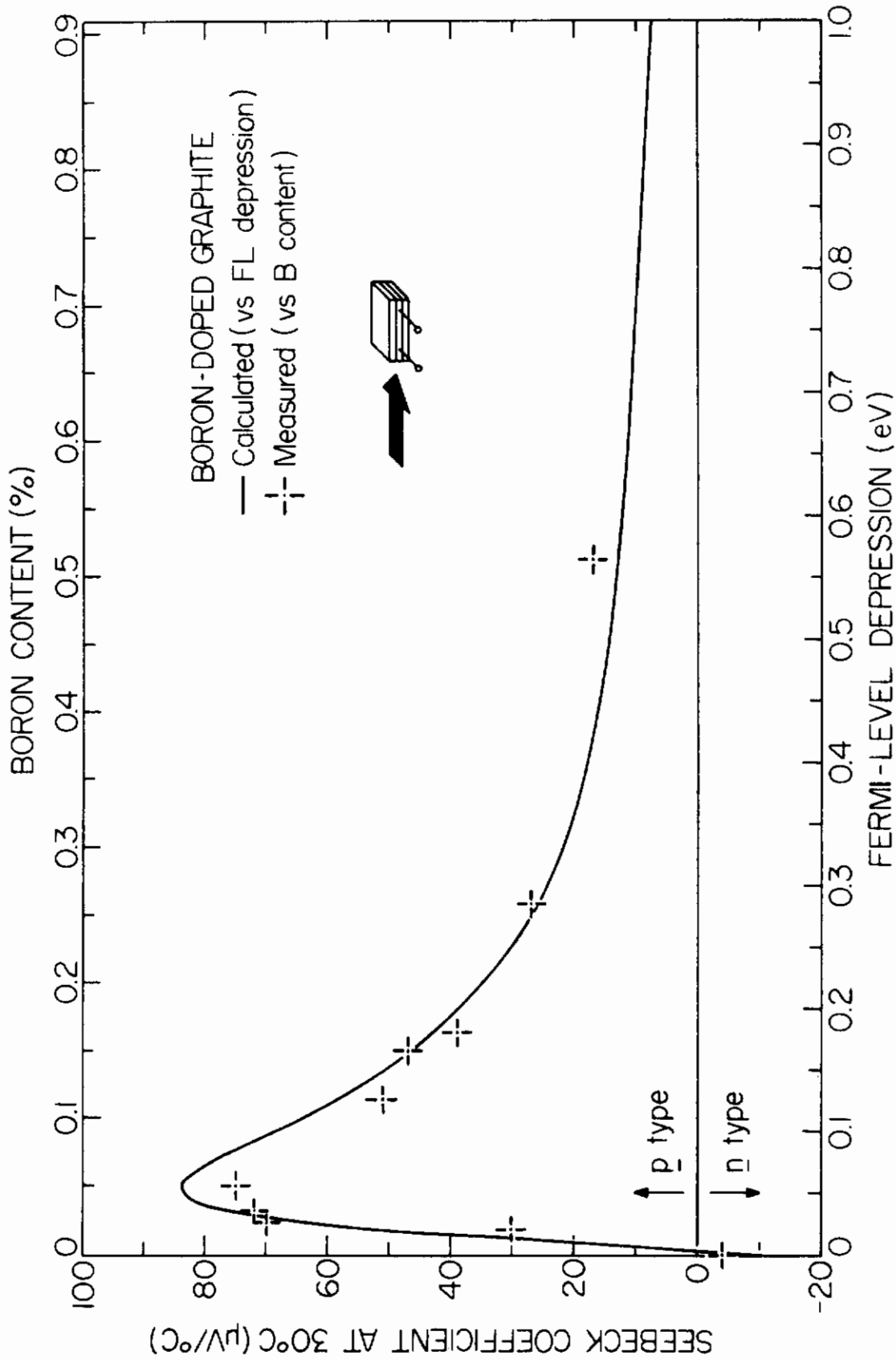
Figure 7   Thermoelectric Power of Graphite at Room Temperature

and thus shows little sensitivity to moderate variations in the Fermi-level position (see Fig. 7). This type of behavior has indeed been observed with various graphites. Thielke and Shepard's[14] measurements on doped polycrystalline graphites, for example, indicate that 0.5 percent B raises the Seebeck coefficient to almost 75 μV/°C, while further boron addition results in a progressive lowering to a level of about 15 μV/°C. In Fig. 5, Thielke and Shepard's data are plotted vs boron content in such a fashion that the peak value at $B/C = 5 \times 10^{-3}$ corresponds to the theoretical maximum at $\Delta = 0.055$ eV. Evidently, our model accounts for the main features of thermoelectricity in pyrolytic graphite.* We also wish to point out that Fig. 7 suggests a simple linear relationship between boron content and Fermi-level depression, namely: B/C (in %) $\approx \Delta$ (in eV).

In the light of this semi-empirical relationship we now may attempt to assess the observed temperature dependence of the Seebeck coefficient of boronated PG specimens. Figure 8 (right-hand side) records data taken on three specimens doped at 0.03, 0.3, and at about 1%. (These numbers are only indicative of the doping level, since chemical analysis reveals appreciable boron-concentration gradients.) On the left-hand side of Fig. 8 are the predicted Seebeck coefficients as derived from (1) with $\underline{b} = 1.1$ throughout the temperature and Δ's as one would expect on the basis of the Fermi level-vs-boron-doping relationship brought forth in Fig. 7. The confrontation shows that, as predicted, lightly doped BPG behaves in a semi-metallic fashion (the Seebeck coefficient decreases with increasing temperature), while heavily doped material exhibits typically metallic characteristics (linear temperature dependence). We may also point out that both the 0.03% and the 1% sample behave strictly in accordance with the calculation; the 0.3% specimen, however, points to Fermi level depressed by substantially more

----

*In Ref. 15 a similar "fit" is presented. We want to emphasize that this early work rests on an inadequate theoretical basis (spherical energy surfaces) and involves the use of $S = -1/2$ (acoustical scattering assumption) which cannot be justified at $\overline{\text{high}}$ boron concentrations.
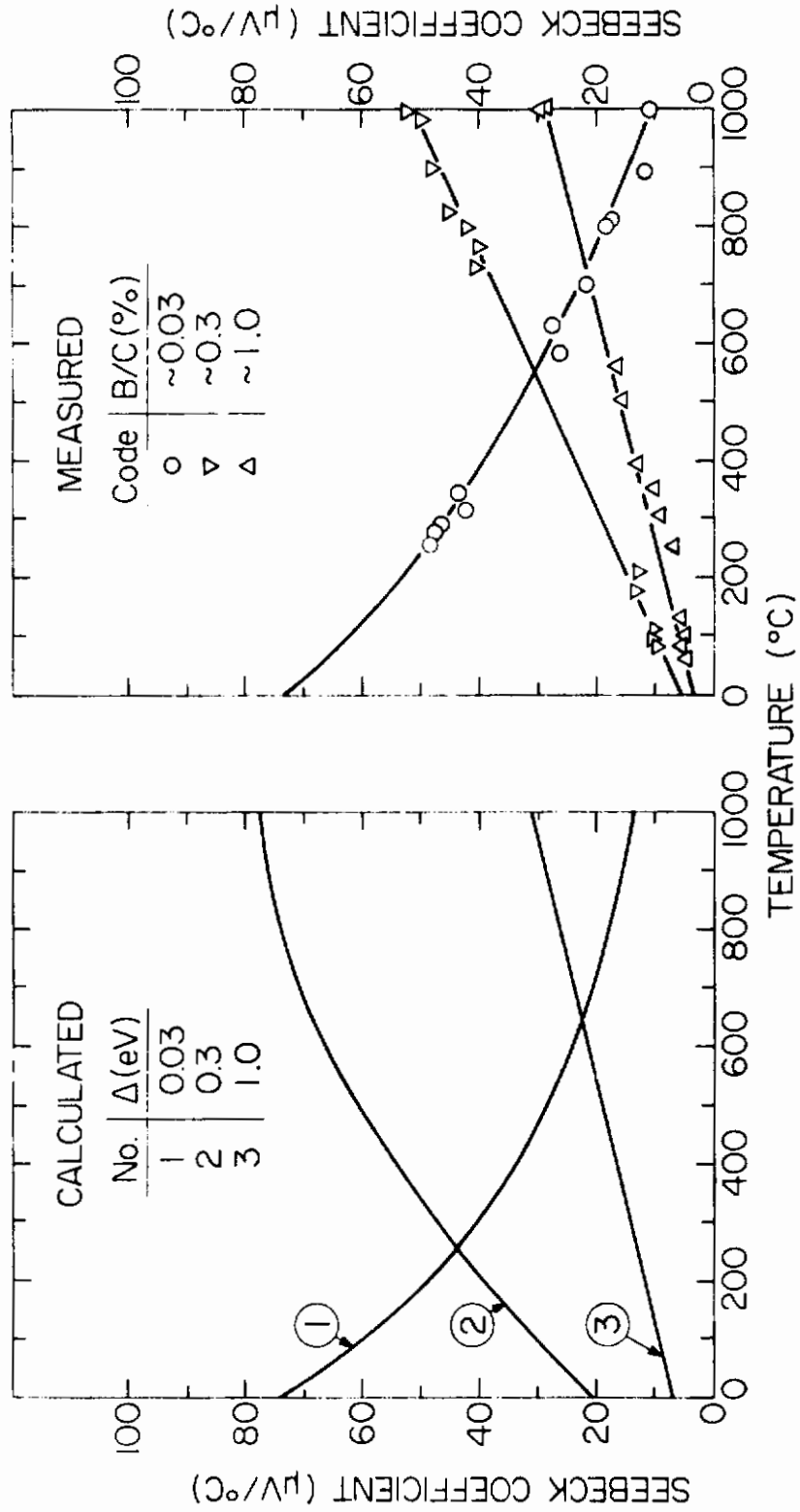
Figure 8   Thermoelectric Power of Three Boron-Doped Pyrolytic
Graphite Specimens in the Temperature Range 0° to 1000°C

than 0.3 eV. A similar phenomenon was observed in connection with Hall-effect studies at high temperature.[13] It may not be ruled out, therefore, that ionization efficiencies (number of free holes per boron atom) vary with the amount of incorporated boron.

Of major significance is the observation that the Seebeck coefficients of heavily doped BPG increases with temperature over the range of relevance to thermocouple work. This accords with the theoretical conclusions stated in Ref.15. In consequence, we now may assert that problems encountered at or above 2000 ℃ are of an experimental nature and involve basic limitations of the furnace instrumentation. In the framework of the present contract we have not been able to cope with the situation.

REFERENCES

1. A. H. Wilson, Theory of Metals (Cambridge University Press, New York, 1954), Chap. 8.

2. J. C. Slonczewski and P. R. Weiss, Phys. Rev. 109, 272 (1958).

3. R. G. Arkhipov, V. V. Kechin, A. K. Likhter, and Y. A. Pospelov, Soviet Physics JETP 17, 1321 (1963).

4. C. A. Klein, J. Appl. Phys. 33, 3338 (1962).

5. J. W. McClure and L. B. Smith, Proceedings of the Fifth Conference on Carbon (Pergamon Press, New York, 1963), Vol. 2, p. 3.

6. R. R. Heikes and R. W. Ure, Thermoelectricity: Science and Engineering (Interscience Publishers, New York, 1961), Chap. 11.

7. W. Thomson, Proceedings of the Royal Society (Edinburgh, December 1851).

8. W. Nernst, Theoretische Chemie (1913), p. 751.

9. G. Borelius, W. H. Keeson, C. H. Johansson, and J. O. Linde, Comm. Leiden, Suppl. No. 70a (1932).

10. J. Nystrom, Arkiv. Mat. Astron. Fysik 34A, No. 27, 1 (1957).

11. N. Cusack and P. Kendall, Proceedings Physical Society 72, 898 (1958).

12. L. C. Blackman, G. Saunders, and A. R. Ubbelohde, Proceedings of the Royal Society A264, 19 (1961).

13. C. A. Klein, M. P. Lepie, W. D. Straub, and S. M. Zalar, Technical Report No. ASD-TDR-63-844 (1963).

14. N. R. Thielke and R. L. Shepard in Technical Report No. TID-7586, pt. 1, p. 44.

15. C. A. Klein and M. P. Lepie, Solid-State Electronics 7, 241 (1964).

DOCUMENT CONTROL DATA - R&D

(Security classification of title, body of abstract and indexing annotation must be entered when the overall report is classified)

1. ORIGINATING ACTIVITY (Corporate author)	2a. REPORT SECURITY CLASSIFICATION
Raytheon Company 28 Seyon Street Waltham, Massachusetts 02154	Unclassified
	2b. GROUP

3. REPORT TITLE

Analysis and Experimental Evaluation of an Ultra-High Temperature
Pyrolytic Graphite Thermocouple

4. DESCRIPTIVE NOTES (Type of report and inclusive dates)

Final Report

5. AUTHOR(S) (Last name, first name, initial)

Klein, C. A.; Lepie, M. P.; Donadio, R. N.

6. REPORT DATE	7a. TOTAL NO. OF PAGES	7b. NO. OF REFS
June 1966	30	15

8a. CONTRACT OR GRANT NO. AF 33(615)-2650 b. PROJECT NO. 1469 c. 146907 d.	9a. ORIGINATOR'S REPORT NUMBER(S) AFFDL-TR-66-27 9b. OTHER REPORT NO(S) (Any other numbers that may be assigned this report)

10. AVAILABILITY/LIMITATION NOTICES This document is subject to special export controls
and each transmittal to foreign governments or foreign nationals may be made only
with prior approval of AF Flight Dynamics Laboratory, Wright-Patterson Air Force
Base, Ohio 45433.

11. SUPPLEMENTARY NOTES	12. SPONSORING MILITARY ACTIVITY Research and Technology Division Wright-Patterson Air Force Base, Ohio 45433

13. ABSTRACT

This report is made up of three segments as follows:

1. A theoretical analysis of thermoelectricity along graphite layer planes.
It is shown how the TEP can be derived from first principles using the
Slonczewski-Weiss description of the graphite band structure. From the density
of state equation we derive rigorous indications on the energy dependence of the
scattering parameter, which allow us to undertake valid comparisons with
experimental results.

2. Chapter II summarizes the experimental procedure. Great care was taken
in order to arrive at reliable Seebeck coefficients. Thermocouple work was
plagued by experimental difficulties (furnace conductance) of a similar nature
as experienced by other investigators.

3. Finally, measured TEP was assessed in the light of the theory developed
in Chap. I. New light is thus shed upon critical parameters such as the mobility
ratio, which leads to a much improved description of transport in pyrolytic
graphite and alloys of pyrolytic graphite. It is demonstrated that BPG/PG
thermocouples are intrinsically capable of delivering exceptionally favorable
output characteristics; a reduction to practice will require further efforts, in
particular in connection with proper test-furnace design.

DD FORM 1473
1 JAN 64

14. KEY WORDS	LINK A		LINK B		LINK C	
	ROLE	WT	ROLE	WT	ROLE	WT
Thermocouples, ultra-high temperature Pyrolytic Graphite Thermoelectricity along graphite layer planes TEP Energy dependence of the scattering parameter						

INSTRUCTIONS

1. **ORIGINATING ACTIVITY:** Enter the name and address of the contractor, subcontractor, grantee, Department of Defense activity or other organization (*corporate author*) issuing the report.

2a. **REPORT SECURITY CLASSIFICATION:** Enter the overall security classification of the report. Indicate whether "Restricted Data" is included. Marking is to be in accordance with appropriate security regulations.

2b. **GROUP:** Automatic downgrading is specified in DoD Directive 5200.10 and Armed Forces Industrial Manual. Enter the group number. Also, when applicable, show that optional markings have been used for Group 3 and Group 4 as authorized.

3. **REPORT TITLE:** Enter the complete report title in all capital letters. Titles in all cases should be unclassified. If a meaningful title cannot be selected without classification, show title classification in all capitals in parenthesis immediately following the title.

4. **DESCRIPTIVE NOTES:** If appropriate, enter the type of report, e.g., interim, progress, summary, annual, or final. Give the inclusive dates when a specific reporting period is covered.

5. **AUTHOR(S):** Enter the name(s) of author(s) as shown on or in the report. Enter last name, first name, middle initial. If military, show rank and branch of service. The name of the principal author is an absolute minimum requirement.

6. **REPORT DATE:** Enter the date of the report as day, month, year; or month, year. If more than one date appears on the report, use date of publication.

7a. **TOTAL NUMBER OF PAGES:** The total page count should follow normal pagination procedures, i.e., enter the number of pages containing information.

7b. **NUMBER OF REFERENCES:** Enter the total number of references cited in the report.

8a. **CONTRACT OR GRANT NUMBER:** If appropriate, enter the applicable number of the contract or grant under which the report was written.

8b, 8c, & 8d. **PROJECT NUMBER:** Enter the appropriate military department identification, such as project number, subproject number, system numbers, task number, etc.

9a. **ORIGINATOR'S REPORT NUMBER(S):** Enter the official report number by which the document will be identified and controlled by the originating activity. This number must be unique to this report.

9b. **OTHER REPORT NUMBER(S):** If the report has been assigned any other report numbers (*either by the originator or by the sponsor*), also enter this number(s).

10. **AVAILABILITY/LIMITATION NOTICES:** Enter any limitations on further dissemination of the report, other than those imposed by security classification, using standard statements such as:

  (1) "Qualified requesters may obtain copies of this report from DDC."

  (2) "Foreign announcement and dissemination of this report by DDC is not authorized."

  (3) "U. S. Government agencies may obtain copies of this report directly from DDC. Other qualified DDC users shall request through

    _____ ."

  (4) "U. S. military agencies may obtain copies of this report directly from DDC. Other qualified users shall request through

    _____ ."

  (5) "All distribution of this report is controlled. Qualified DDC users shall request through

    _____ ."

If the report has been furnished to the Office of Technical Services, Department of Commerce, for sale to the public, indicate this fact and enter the price, if known.

11. **SUPPLEMENTARY NOTES:** Use for additional explanatory notes.

12. **SPONSORING MILITARY ACTIVITY:** Enter the name of the departmental project office or laboratory sponsoring (*paying for*) the research and development. Include address.

13. **ABSTRACT:** Enter an abstract giving a brief and factual summary of the document indicative of the report, even though it may also appear elsewhere in the body of the technical report. If additional space is required, a continuation sheet shall be attached.

It is highly desirable that the abstract of classified reports be unclassified. Each paragraph of the abstract shall end with an indication of the military security classification of the information in the paragraph, represented as (TS), (S), (C), or (U).

There is no limitation on the length of the abstract. However, the suggested length is from 150 to 225 words.

14. **KEY WORDS:** Key words are technically meaningful terms or short phrases that characterize a report and may be used as index entries for cataloging the report. Key words must be selected so that no security classification is required. Identifiers, such as equipment model designation, trade name, military project code name, geographic location, may be used as key words but will be followed by an indication of technical context. The assignment of links, rules, and weights is optional.